Kinetics of mixed succinic acid/acetic acid esterification with Amberlyst 70 ion exchange resin as catalyst

Alvaro Orjuela [a,b], Abraham J. Yanez [a], Arati Santhanakrishnan [a], Carl T. Lira [a], Dennis J. Miller [a,*]

[a] Department of Chemical Engineering & Materials Science, Michigan State University, 2527 Engineering Building, East Lansing, MI 48824, United States
[b] Universidad Nacional de Colombia, Ciudad Universitaria, Dept. de Ingeniería Química. Bogotá DC, Colombia

ARTICLE INFO

ABSTRACT

Liquid phase esterification of succinic acid, acetic acid and succinic/acetic acid mixtures with ethanol was studied using Amberlyst 70 strong cation exchange resin as catalyst. Batch isothermal reactions were performed at different ethanol:acid molar ratios (1:1–27:1), temperatures (343–393 K) and catalyst loadings (1.0–9.3 wt% of solution). Esterification kinetics is described using both pseudo-homogeneous mole fraction and NRTL-based activity based models that take ethanol dehydration to diethyl ether into account. The models accurately predict the esterification of individual acids, and a simple additive combination of independent kinetic models provides a good description of mixed acid esterification. The kinetic models can be used in simulation of reactive distillation processes for mixed acid esterification.

© 2012 Elsevier B.V. All rights reserved.

1. Introduction

Among several carboxylic acids obtained by fermentation, succinic acid (1,4-butanedioic acid, herein succinic acid (SA)) has been recognized as a renewable platform molecule for many chemical derivatives of industrial interest [1–6]. Its potential use as feedstock for 1,4-butanediol, tetrahydrofuran and γ-butyrolactone production opens the opportunity for a growing and sustainable market of renewable polymers [7,8]. Because SA is a common metabolite in many anaerobic and facultative microorganisms, a number of promising fermentation processes have been developed using bacteria isolated from gastrointestinal systems in animals, including *Anaerobiospirillum succinicipro-ducens* (~50 kg/m³), *Actinobacillus succinogenes* (94-106 kg/m³), *Mannheimia succiniciproducens* (~52 kg/m³), and *Escherichia coli* (~99 kg/m³) [9–12].

Two major challenges in SA fermentation are achieving high SA titer (g/l) and avoiding loss of selectivity via byproduct formation. In addition to cell growth and incomplete conversion, sugar substrate is lost via formation of significant quantities of acetic, formic, pyruvic, and lactic acids depending on the organism. Typical acid concentrations found in SA fermentation broths are listed in Table 1.

According to recent studies, recovery of succinic acid from these mixtures can be accomplished by esterification with ethanol

(EtOH). Succinate and other carboxylic acid salts can react directly with EtOH using sulfuric acid as an acidulant and catalyst. A mixture of free acid and esters in EtOH is produced, while sulfate salts are removed by precipitation. The ethanolic solution is fed into a reactive distillation column for complete esterification and selective separation of esters [13].

Esterification of SA proceeds sequentially through two reactions in series in the presence of an acid catalyst, with monoethyl succinate (MES) as intermediate and diethyl succinate (DES) as final product (Fig. 1). Because of chemical equilibrium limitations in esterification and the low solubility of SA in ethanol (~10% by weight at 298 K), excess EtOH is required in reaction. Further, achieving high rates and overcoming chemical equilibrium limitations requires continuous water (H₂O) removal, thus making esterification an attractive reaction system for reactive distillation (RD). For esterification of carboxylic acids, a single continuous RD column can selectively separate either product water or ester from the acid reactant as it is formed. In this way, even dilute acid solutions produced via fermentation [14–16] can be directly esterified to obtain esters as high purity products.

In SA esterification, it is not known whether the presence of byproduct acids (Table 1) accelerates or inhibits SA conversion, or whether formation and recovery of byproduct acid esters overcomplicates the recovery process. As part of our efforts to develop RD strategies for succinic acid esterification, we have carried out this study of esterifying mixtures of SA and acetic acid (AcAc), the byproduct in greatest concentration in SA fermentation (Table 1), with ethanol (EtOH) for the purpose of understanding

* Corresponding author. Tel.: +1 517 353 3928.
  E-mail address: millerd@egr.msu.edu (D.J. Miller).

Nomenclature

AcAc	acetic acid
a_{ij}	binary energy parameter in NRTL equation for pair ij
b_{ij}	binary parameter for NRTL equation for pair ij (K)
C_i	concentration of component i in the bulk phase (kmol/m^3)
C_T	total molar concentration in liquid phase (kmol/m^3)
C_{SA}	concentration of SA in the bulk phase (kmol/m^3)
DEE	diethyl ether
D_{eff}	effective diffusivity of SA inside the catalyst pores (m^2/s)
D_{SA}	molecular diffusivity of SA in liquid phase (m^2/s)
DES	diethyl succinate
d_P	catalytic particle diameter (m)
$E_{a,m}$	energy of activation of forward reaction m (kJ/kmol)
EtOH	ethanol
EtAc	ethyl acetate
f_{ABS}	sum of absolute differences (objective function in regression)
G_{ij}	binary parameter for NRTL equation for pair ij
$K_{a,m}$	equilibrium constant for reaction m, activity basis
$K_{x,m}$	equilibrium constant for reaction m, mole fraction basis
$K_{\gamma,m}$	activity coefficient ratio for reaction m
$k_{0,m}$	pre-exponential factor of forward reaction m (kmol/kg$_{CAT}$ s)
MES	monoethyl succinate
MW	molecular weight of component i (kg/kmol)
N_i	number of moles of component i (kmol)
N_T	total number of moles (kmol)
n	number of experimental samples
r_m	rate of reaction per volume of liquid in reaction m (kmol/m^3 s)
$r_m^{\dagger}$	rate of reaction per mass of catalyst in reaction m (kmol/kg$_{CAT}$ s)
R	ideal gas constant (kJ/mol K)
SA	succinic acid
t	time (s)
T	temperature (K)
V	reaction volume (m^3)
V_P	catalytic particle volume (m^3)
w_{CAT}	catalyst loading (kg$_{CAT}$/kg solution)
x_i	mole fraction of component i

Greek letters

α_{ij}	non-randomness parameter of NRTL equation
ε	porosity of solid catalyst
ϕ	Thiele modulus
γ_i	activity coefficient of component i
μ_{liquid}	viscosity of liquid phase (cP)
η	effectiveness factor
ρ_{CAT}	density of the catalyst (kg/m^3)
ρ_{sol}	density of the liquid solution (kg/m^3)
τ	tortuosity of solid catalyst
τ_{ij}	binary parameter of NRTL equation
$\theta_{i,m}$	ratio of stoichiometric coefficients of component i to the reference component in reaction m
Φ_w	Weisz–Prater modulus
ν_i	stoichiometric coefficient of component i

Subscripts and superscripts

ABS	absolute
Avg	average
EQ	equilibrium
dry	dry state of the catalyst
Calc	calculated data
Exp	experimental data
i	component identification
Obs	observed
m	reaction identification
N_C	number of components
Sol	solution
swollen	swollen state of the catalyst

Table 1
Typical product concentrations in SA fermentation [12].

Component	Concentration (kg/m^3)
Succinic acid	40–110
Acetic acid	5–40
Pyruvic acid	0–20
Lactic acid	0–14
Formic acid	0–5

how AcAc affects SA esterification under process-relevant conditions.

In recent papers [17–19] it has been demonstrated that the strong cation exchange resin Amberlyst 70®, a low cross linked sulfonated and chlorinated styrene-divinylbenzene resin, showed superior performance (e.g. higher turnover frequency) as an acid catalyst relative to the more commonly used macroreticular ion exchange resins (e.g. Amberlyst 15) that are only sulfonated. The high temperature stability of Amberlyst 70 (up to 443 K in most environments) [19,20] also makes it more attractive for use in reactive distillation, where high reaction rates and thus elevated temperatures are required for efficient column operation [21,22].

While there are reports of SA [21,22] and AcAc [23–29] esterification with EtOH using ion exchange resins, none have used Amberlyst 70 as catalyst. We thus have measured and report here the kinetics of AcAc and SA esterification, both individually and in mixtures, over Amberlyst 70 resin. In addition to ester formation, dehydration of EtOH to diethyl ether (DEE) occurs at elevated temperatures, so we include it as an integral part of the kinetic model. The kinetics of mixed acid esterification, along with associated physical property and phase equilibrium data, are useful in designing reactive distillation systems for fermentation-derived SA esterification.

2. Material and methods

2.1. Materials

Succinic acid (>99.5%, Sigma–Aldrich), acetic acid (99.9%, Aristar), diethyl succinate (99.92%, Sigma–Aldrich), monoethyl succinate (89.3%, Sigma–Aldrich), ethyl acetate (HPLC grade, J.T. Baker), ethanol (200 proof, Decon Labs), water (HPLC grade, J.T. Baker), diethyl ether (99.9%, EMD chemicals) n-butanol (99.9%, Mallinckrodt), and acetonitrile (HPLC grade, EMD) were used without further purification for experiments and calibrations. Species purity was confirmed by gas chromatography; no impurities, other than small amounts of water, were detected in appreciable concentrations. Hydranal-coulomat E solution (Riedel-de Haën) was used in Karl–Fisher analysis for water measurement. Amberlyst 70® resin was purchased from Dow Chemical Company; its physical and chemical properties are listed in Table 2.
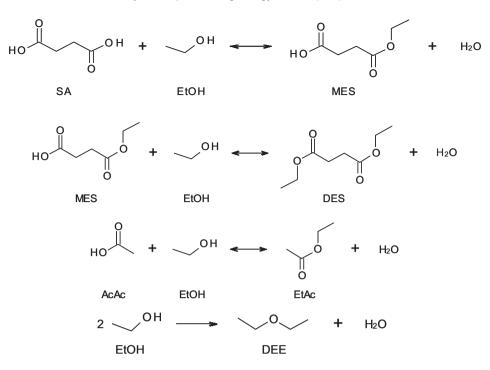
Fig. 1. Reactions: esterification of succinic acid (SA) to monoethyl succinate (MES) and diethyl succinate (DES); esterification of acetic acid (AcAc) to ethyl acetate (EtAc); dehydration of EtOH to diethyl ether (DEE).

Table 2
Physical and chemical properties of Amberlyst 70® [17–20].

Physical form	Dark spherical beads
Ionic form	H^+
Acid equivalents (eq/kg dry solid)	≥ 2.55
Surface area (N_2 – BET) (m^2/g)	31–36
Average pore diameter (Å)	195–220
Effective size – dry solid (mm)	0.5
Pore volume (m^3/kg)	$1.5–3.3 \times 10^{-4}$
Particle porosity	0.19
Uniformity coefficient	≤ 1.5
Skeletal density (kg/m^3)	1520
Swollen surface area (ISEC)[a] (m^2/g)	176
Swollen particle porosity (water) (ε)	0.57
Maximum operating temperature (K)	463

[a] ISEC = inverse steric exclusion chromatography [17].

2.2. Experimental procedures

2.2.1. Catalyst conditioning

As-received Amberlyst 70 resin contained a range of particle sizes and was thus sieved in a series of US-standard sieves (Dual Manufacturing Co.). The −45 + 60 mesh (0.25–0.35 mm diameter) fraction was used in kinetic experiments unless otherwise specified. The resin was rinsed initially with water, followed by several washing cycles with ethanol. After filtration and removal of excess liquid, the catalyst was dried at 353 K under vacuum (1 kPa) and then stored in a sealed container in a vacuum oven prior to use.

The ion exchange capacity of dry Amberlyst 70 was measured by titration with a 0.1 M solution of NaOH in water using phenolphthalein as the indicator. The acid site density, obtained as the average of three measurements, was 2.35 ± 0.1 eq/kg, a value slightly lower but in reasonable agreement with the value of 2.55 eq/kg reported by the manufacturer [20].

2.2.2. Batch kinetic experiments

Isothermal batch kinetic experiments were performed in a Parr 5000 Multireactor® system (Parr Instrument Co., Moline, Illinois) that includes six 75 cm^3 stainless steel reactors equipped with magnetic stirrer, temperature control, and sampling system with a stainless steel frit on the sampling tube to avoid withdrawal of catalyst. Ethanol, AcAc, and SA were placed into each reactor at room temperature in predetermined molar ratios along with the specified quantity of catalyst; the total mass of reactants added was typically 0.050 kg. After sealing each reactor, the stirring rate was set at 900 rpm and heating was initiated. It typically took 15 min to reach the desired reaction temperature; this moment was taken as time zero ($t = 0$) of reaction. During reaction, 0.25–0.5 cm^3 samples were withdrawn with a syringe connected to a sampling port at specified time intervals starting at $t = 0$, with a higher frequency of sampling in the first 2–3 h. Samples were transferred into hermetically sealed vials and stored in a refrigerator before analysis.

2.3. Analysis

Reaction samples were analyzed both by gas and liquid chromatography. For HPLC, samples were diluted 50-fold in water and analyzed in a system consisting of a Waters® 717 autosampler, a Waters® 410 refractive index detector, and a PerkinElmer LC90 UV detector. A 100 mm × 7.6 mm Fast Acid analysis column (BioRad®) at 298 K along with a mobile phase of 5 mM H_2SO_4 in water flowing at 1.0 ml/min was used for the separation. Because the retention times of EtOH and MES were similar, only UV detection was used to evaluate MES concentration.

To evaluate concentration of volatile components, samples were diluted 20-fold into acetonitrile containing 5.0 wt% n-butanol as an internal standard and analyzed on a gas chromatograph (HP 5890 Series II) equipped with thermal conductivity and flame ionization detectors. A 30 m long Alltech Aqua WAX-DA column (0.53 mm i.d., 1.20 μm film thickness) was used with the following temperature program: initial temperature 313 K for 3 min; ramp at 20 K/min to 523 K, and hold at 523 K for 0.5 min. The GC injection port was maintained at 543 K in a splitless mode, and detector temperature was 523 K. Helium was used as carrier gas (0.25 cm^3/s) and liquid injection volumes of 0.5 μL were used.

For both analyses, standard samples of known composition in the range of interest were injected in triplicate to obtain calibration curves repeatable to within ±0.5% by mass.

Karl–Fisher analysis (Aquacount coulometric titrator AQ-2100) was used to measure water content in reagents and samples.

3. Results and discussion

A preliminary set of three experiments was carried out under identical conditions (Catalyst loading = 0.011 kg/kg solution; mole ratio EtOH:SA = 7.5:1; T = 353 K) to characterize repeatability of the kinetic measurements. For samples taken at identical times in the three experiments, the mean deviation in species concentration from the experimental average was approximately 4%. This uncertainty can be largely attributed to measurement of succinate species concentrations below 1 wt% in solution. The complete set of batch experiments carried out to characterize the reactions involved in this study is given in Table S1: ethanol dehydration to diethyl ether (DEE) was studied in Runs 1–11; SA esterification was examined in Runs 11–51; AcAc esterification was evaluated in Runs 52–83; and finally mixed SA/AcAc esterification experiments were carried out in Runs 84–88. In these experiments, the Amberlyst 70 catalyst loadings used (0.5–9.3 wt%) correspond to the equivalent acidity of 0.1–2.0 wt% H_2SO_4 in solution.

3.1. Mass transfer considerations

Preliminary SA esterification experiments in which agitation speed was varied showed nearly identical conversion rates at all speeds above 500 rpm, indicating that no external liquid–solid mass transfer resistances are present. Evaluation of intraparticle mass transfer effects is carried out by estimating the observable modulus (Φ_w) and invoking the Weisz–Prater criterion [31]. For a spherical particle

$$\Phi_w = \frac{\left(r^\dagger_{\text{Obs}}\right) \rho_{\text{CAT}}(d_P/6)^2}{D_{\text{eff}}C_{\text{SA}}} \tag{1}$$

here $r^\dagger_{\text{Obs}}$ is the observed rate of reaction per mass of catalyst, ρ_{CAT} and d_P are the catalyst particle density and diameter, respectively, at reaction conditions (e.g., the swollen particle state in EtOH), D_{eff} is the effective diffusivity of SA in the catalyst, and C_{SA} is the concentration of SA in the bulk liquid. Reaction rate $r^\dagger_{\text{Obs}}$ can be calculated as

$$r^\dagger_{\text{Obs}} = \frac{r_{\text{Obs}}}{w_{\text{CAT}}\rho_{\text{Sol}}} \tag{2}$$

where r_{Obs} is the rate of reaction per unit volume of reacting phase (liquid) obtained from the slope of the SA concentration vs. time curve, w_{CAT} is the mass of catalyst per mass of reacting phase, and ρ_{Sol} is density of the reacting phase.

A simple measurement showed that the swelling ratio (swollen volume V_{Pswollen} divided by dry volume V_{Pdry}) of Amberlyst 70 catalyst was 2.0 in EtOH. Assuming homogeneous swelling of the spherical particles, the actual particle diameter is calculated as

$$d_P = d_{\text{Pdry}} \times \sqrt[3]{\frac{V_{\text{Pswollen}}}{V_{\text{Pdry}}}} \tag{3}$$

Taking the average particle diameter of dry solids used in experiments as 0.30 mm, a swelled particle diameter of 0.37 mm is obtained. Because liquid absorption gives Amberlyst 70 porosity similar to macroreticular resins [17–19], the swelled particle density is assumed 1000 kg/m³ as reported previously for EtOH absorption in Amberlyst 15 [30]. The effective diffusivity (D_{eff}) is estimated from the liquid-phase diffusion coefficient (D_{SA})

Table 3
Evaluation of mass transfer resistances at initial reaction conditions using the Weisz–Prater criterion.

w_{CAT} (kg$_{\text{CAT}}$/kg$_{\text{sol}}$)	0.011	
ρ_{Sol} (kg/m³)	770	
C_{SA} (solution) (kmol/m³)	0.67	
d_{Pswollen} (mm)	0.37	
ρ_{CAT} (kg/m³)	1000	
EtOH association factor for Wilke–Chang model	1.5	
SA molar volume at T_B (cm³/mol)	83.58	
Experiment Run #	26	28
T (K)	353	379
μ_{liquid} (cP)	0.56	0.39
D_{SA} (m²/s)	2.7×10^{-9}	4.2×10^{-9}
D_{eff} (m²/s)	8.9×10^{-10}	1.36×10^{-9}
$r^\dagger_m$ (kmol/kg$_{\text{CAT}}$) (1/s)	2.0×10^{-5}	3.7×10^{-5}
Φ_w	0.13	0.17
ϕ	0.37	0.42
η	0.95	0.94

computed via the Wilke–Chang equation and by assuming pore tortuosity (τ) is the inverse of particle porosity (ε) [30]. The effective diffusivity of SA is thus given by

$$D_{\text{eff}} = D_{\text{SA}}\left(\frac{\varepsilon}{\tau}\right) = D_{\text{SA}}\varepsilon^2 \tag{4}$$

The Thiele modulus (ϕ) and effectiveness factor (η) for SA esterification can be calculated from the observable modulus if it is assumed the reaction is pseudo-first order in SA because of the large excess of EtOH present.

$$\Phi_w = \eta\phi^2 \tag{5}$$

where

$$\eta = \frac{\tanh\phi}{\phi} \tag{6}$$

Values of Φ_w calculated for an initial EtOH:SA molar ratio of 22:1 ($x_{\text{SA}} = 0.042$) and at two temperatures are presented in Table 3. From these values, the first-order effectiveness factor for each of these experiments is ∼0.95, indicating that internal mass transfer resistances play a minor role in SA esterification [31]. Similar calculations likewise indicate minimal influence of diffusion in AcAc esterification and dehydration of EtOH to DEE.
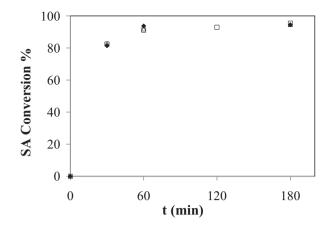
To further investigate intraparticle mass transfer, Amberlyst 70 catalyst was sieved into three fractions. First, particles larger than 35 mesh (>500 μm) were collected in the sieve tray. Smaller particles were ground and collected in two additional fractions: the −35 + 60 mesh fraction (250–500 μm) and a −100 mesh fraction (<150 μm). Ion exchange capacity was measured in each fraction; no change in acidity was observed as a result of the grinding process.

Esterification experiments were run at identical conditions with the three different Amberlyst 70 catalyst particle sizes. Results are presented in Fig. 2; no difference in the rate of reaction was observed for the different catalyst particle sizes at these conditions.

3.2. Reaction equilibrium constants

Equilibrium constants for the esterification reactions were measured by running experiments for long time periods (>23 h). The equilibrium constants ($K_{a,m}$) for each reaction were calculated using the experimental mole fractions and liquid-phase activity coefficients at equilibrium of each of the N_C components of the reaction:

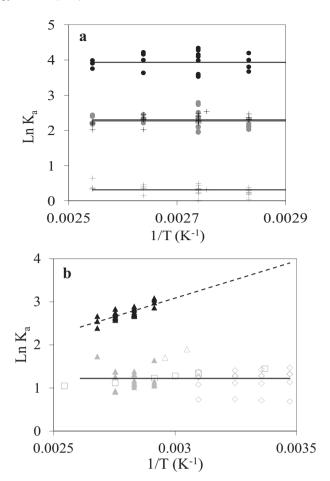$$K_{a,m} = K_{x,m}K_{\gamma,m} = \prod_{i=1}^{N_C}(x_i\gamma_i)^{\nu_i}_{\text{EQ}} \tag{7}$$

Fig. 2. Esterification of SA with EtOH over different particle sizes of Amberlyst 70: (●) $d_P < 150\,\mu$m; (□) $250\,\mu$m $< d_P < 590\,\mu$m; (△) $d_P > 590\,\mu$m. $w_{CAT} = 0.044$; mole ratio EtOH:SA = 7.5:1; $T = 353$ K.

here x_i, γ_i and ν_i are the mole fraction, activity coefficient, and stoichiometric coefficient of component i in the reactive mixture, respectively. The ratio of activity coefficients $K_{\gamma,m}$ accounts for deviations from ideal behavior of the mixture. At 383 K, the irreversible formation of diethyl ether (DEE) precluded establishment of a clear equilibrium condition, so experiments at this temperature were not included in equilibrium constant calculations.

The NRTL equation was used to evaluate activity coefficients of components in the reaction mixture because of its ability to simultaneously represent vapor–liquid, liquid–liquid, and solid–liquid equilibria [32–38]. Some binary interaction parameters in the NRTL model were obtained from literature or from the AspenPlus (Version 7.1, AspenTech, Inc.) database [33,34]; others were determined by vapor–liquid equilibrium and liquid–liquid equilibrium measurements in our laboratory [35–38]. Parameters for H_2O–DEE, EtOH–DEE, AA–DEE and EtAc–DEE were regressed from reported vapor–liquid and liquid–liquid phase equilibria data using the regression tool in AspenPlus [33]. Plots of binary and ternary phase equilibrium data, along with fitted predictions, are presented in Fig. S1 of the Supplementary Material. The list of binary interaction parameters used in calculation of activity coefficients is presented in Table S2 of the Supplementary material.

The experimental values of mole fraction- and activity-based equilibrium constants for SA and AcAc esterification are presented in a Van't Hoff plot in Fig. 3. The values agree with those reported in the literature under similar conditions [21,22,27,34] as seen in Figure 3 for acetic acid esterification. The difference between activity- and mole fraction-based equilibrium constants reflects the significant non-ideality of the system ($K_\gamma \sim 4$–7). From these data, optimum values of equilibrium constants for each reaction were determined by linear regression and are reported in Table 4. As seen in Fig. 3a, there is little dependence of the SA esterification equilibrium constants on temperature, so the heats of reaction can be taken as zero. Fig. 3b suggests that the activity-based equilibrium constant for ethyl acetate formation decreases with increasing temperature. From the slope of $\ln(K_a)$ vs. $1/T$ (dotted line in Fig. 3), the estimated heat of reaction for ethyl acetate formation is -13.8 kJ/mol, a value consistent with that obtained for the reaction over similar catalysts [26,28]. However, for the kinetic model of acetic acid esterification we did not include this temperature dependence but instead used an average value of the equilibrium constant reported in Table 4.

Table 4 also includes the 95% confidence intervals for the equilibrium constants. The confidence intervals were determined in a final, simultaneous regression analysis of all kinetic and equilibrium constants using the Nlpredci in Matlab 7.12.0, taking the

Fig. 3. Mole fraction- (gray) and activity- (black) based esterification equilibrium constants from experimental data. (a) Succinic acid esterification: (●, ●) K_1: (+, +) K_2 (reported values for mole fraction are $\ln(K_{x,1}) = 1.66$ and $\ln(K_{x,2}) = 0.182$ [21]) (b) acetic acid esterification: (▲, ▲) this work; (◇) Darlington et al. [22]; (△) Hangx et al. [26]; (□) Tang et al. [34].

Table 4
Optimized parameters with 95% confidence intervals for pseudo-homogeneous kinetic models.

Parameter	Mole fraction	Activity
SA esterification		
$k_{a,1}$ (kmol/kg$_{CAT}$/s)	2870 ± 260	2540 ± 250
$E_{a,1}$ (kJ/kmol)	$51,100 \pm 200$	$67,700 \pm 200$
$K_{a,1}$	9.0 ± 0.1	34.7 ± 0.2
$k_{a,2}$ (kmol/kg$_{CAT}$) (1/s)	$161,000 \pm 11,000$	$37,000 \pm 12,000$
$E_{a,2}$ (kJ/kmol)	67700 ± 300	$63,000 \pm 1100$
$K_{a,2}$	1.3 ± 0.1	10.2 ± 0.6
AcAc esterification		
$k_{a,3}$ (kmol/kg$_{CAT}$) (1/s)	$12,500 \pm 200$	3660 ± 40
$E_{a,3}$ (kJ/kmol)	$56,700 \pm 200$	$52,300 \pm 200$
$K_{a,3}$	3.0 ± 0.1	12.5 ± 0.1
EtOH dehydration		
$k_{a,4}$ (kmol/kg$_{CAT}$) (1/s)	340 ± 329	185 ± 188
$E_{a,4}$ (kJ/kmol)	$78,400 \pm 3200$	$76,600 \pm 3400$

values in Table 4 as initial estimates. The final regressed values were the same as those determined from Fig. 3.

The scatter in the equilibrium constants seen in Fig. 3 is attributed primarily to analytical uncertainty, because calculation of the equilibrium constant requires values for all species concentrations that typically must be determined by several different means. Uncertainty in the equilibrium constant was greater at large excess of EtOH, where nearly complete SA or

AcAc conversion was obtained and low concentrations of residual acids were difficult to accurately measure. Further, a prior study of esterification equilibrium over ion exchange resin catalysts [22] reports that selective absorption of reacting components inside the catalyst particles changes the bulk liquid concentration and thus the value of the calculated equilibrium constant. This would affect the mole fraction-based calculation but not the activity-based equilibrium constant, as activity at equilibrium will be the same inside and outside of the catalyst particles. But despite the scatter in experimental values, the 95% confidence intervals for the equilibrium constants in Table 4 are a small percentage of the constant's value because of the large number of data points collected at near equilibrium conditions during experiments.

3.3. Kinetic model description

In a batch reactor, the change in number of moles N_i of component i participating in m reactions can be expressed as

$$\frac{dN_i}{dt} = N_T \frac{dx_i}{dt} = \left(\sum_{m=1}^{m} \theta_{i,m} r_m \right) V \tag{8}$$

here N_T is the total number of moles in the reactor, V is the reaction volume, r_m is the rate of reaction m per unit volume, and x_i is the mole fraction of component i in the liquid mixture. The parameter $\theta_{i,m}$ is the ratio of stoichiometric coefficients of component i with respect to the reference component in reaction m.

Eq. (8) can be expressed in terms of total molar concentration in the liquid phase $C_T (V/N_T = 1/C_T)$ calculated from average molecular weight (MW_{Avg}) and the density of the solution.

$$\frac{dx_i}{dt} = \frac{1}{C_T} \left(\sum_{m=1}^{m} \theta_{i,m} r_m \right) = \frac{MW_{Avg}}{\rho_{Sol}} \left(\sum_{m=1}^{m} \theta_{i,m} r_m \right) \tag{9}$$

Preliminary experiments confirmed that rates of reaction are linearly dependent on the catalyst loading (w_{CAT}) (Fig. 4); this is further evidence of the intrinsic nature of the reaction rate data collected.

Using a pseudo-homogeneous model for the reversible esterification reactions, the rate of reaction of SA with EtOH can be expressed as
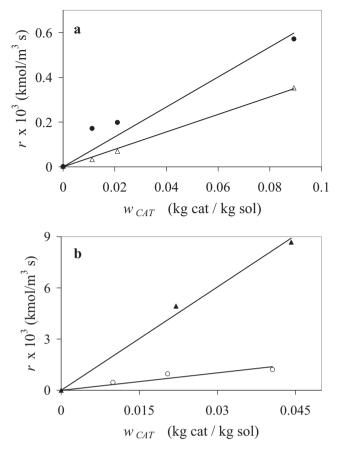
$$r_1 = w_{CAT} \rho_{Sol} k_{0,1} \exp \left(\frac{-E_{a,1}}{RT} \right)$$
$$\times \left[(x_{SA} \gamma_{SA})(x_{EtOH} \gamma_{EtOH}) - \frac{(x_{MES} \gamma_{MES})(x_{H_2O} \gamma_{H_2O})}{K_{a,1}} \right] \tag{10}$$

Using the same approach for the second step of SA esterification (Fig. 1), the rate of formation of DES is described by

$$r_2 = w_{CAT} \rho_{Sol} k_{0,2} \exp \left(\frac{-E_{a,2}}{RT} \right)$$
$$\times \left[(x_{SA} \gamma_{SA})(x_{EtOH} \gamma_{EtOH}) - \frac{(x_{MES} \gamma_{MES})(x_{H_2O} \gamma_{H_2O})}{K_{a,2}} \right] \tag{11}$$

here $k_{0,m}$ and $E_{a,m}$ represent the pre-exponential factor and the energy of activation of the forward reaction m, respectively. The equilibrium constant of reaction m, $K_{a,m}$, is the ratio of forward and reverse rate constants. Similarly, the rate of AcAc esterification with EtOH can be expressed as

$$r_3 = w_{CAT} \rho_{Sol} k_{0,3} \exp \left(\frac{-E_{a,3}}{RT} \right)$$
$$\times \left[(x_{AcAc} \gamma_{AcAc})(x_{EtOH} \gamma_{EtOH}) - \frac{(x_{EtAc} \gamma_{EtAc})(x_{H_2O} \gamma_{H_2O})}{K_{a,3}} \right] \tag{12}$$

Fig. 4. Initial reaction rate at different catalyst loadings. (a) SA esterification at $T = 353$ K, EtOH:SA = 23:1. (●) r_1; (△) r_2. (b) (○) AcAc esterification (r_3) at $T = 353$ K, EtOH:AcAc = 7.5:1; (▲) EtOH dehydration to DEE (r_4) at $T = 393$ K.
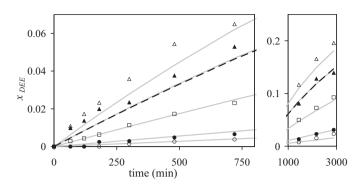
Considering that EtOH dehydration is irreversible, the rate of DEE formation can be expressed as

$$r_4 = w_{CAT} \rho_{Sol} k_{0,4} \exp \left(\frac{-E_{a,4}}{RT} \right) [(x_{EtOH} \gamma_{EtOH})^2] \tag{13}$$

3.4. Determination of rate constants

Substituting Eqs. (10)–(13) into Eq. (9) for each component gives a set of ordinary differential equations to be solved simultaneously as a mixed acid esterification model. Two forms of this model were fit to the experimental data: the first activity-based, with activity coefficients in all rate expressions, and the second a simplified mole fraction form generated by setting all activity coefficients in Eqs. (10)–(13) equal to 1.0. As previously mentioned, esterification mixtures are non-ideal and activity coefficients can change drastically with composition during reaction (e.g. transition from a homogeneous to a multiphase system), so the activity-based model is warranted for this system. The mole fraction-based model, while not rigorous in its depiction of the physical system, is included because it is readily applied and useful for preliminary design.

In the complete mixed SA + AcAc esterification model with DEE formation, there are 11 possible adjustable parameters: four pre-exponential factors, four activation energies, and three equilibrium constants. To simplify the parameter fitting and ultimately investigate interdependence of the reactions, the kinetic constants for EtOH dehydration to DEE (Runs 1–11) were first regressed (Table 4). Using these values and values of the equilibrium constants determined by earlier regression of equilibrium data (Table 4), the kinetic parameters for SA esterification (Runs 12–51) and AcAc esterification (Runs 52–83) were then determined in separate regressions.

Fig. 5. Experimental and predicted mole fraction profiles in DEE formation. (○) Run 1: $T = 363$ K, $w_{CAT} = 0.08$; (□) Run 3: $T = 388$ K, $w_{CAT} = 0.081$; (△) Run 4: $T = 403$ K, $w_{CAT} = 0.08$; (●) Run 5: $T = 363$ K, $w_{CAT} = 0.16$; (▲) Run 7: $T = 388$ K, $w_{CAT} = 0.16$. (━━) Activity based model; (━━) mole fraction model.

Because many of the experiments performed on the individual acids reached chemical equilibrium relatively quickly, only those Runs for each acid that had two or more data points in the kinetic regime (e.g. apart from equilibrium) were used in the regression. These runs are identified in Table S3.

Using the designated kinetic experiments, rate constant parameters for each reaction were determined by numerically integrating Eq. (9) for each component via a fourth order Runge–Kutta method using the differential equation solver ode23 in Matlab 7.12.0. Optimization of kinetic parameters was performed using Nlinfit in Matlab 7.12.0 by minimizing the sum of absolute differences between experimental (x_{i-Exp}) and calculated (x_{i-Calc}) species mole fractions via the objective function given in Eq. (14).

$$f_{ABS} = \frac{1}{n} \sum_{samples} \sum_{i=1}^{N_C} \left| x_{i-Exp} - x_{i-Calc} \right| \qquad (14)$$
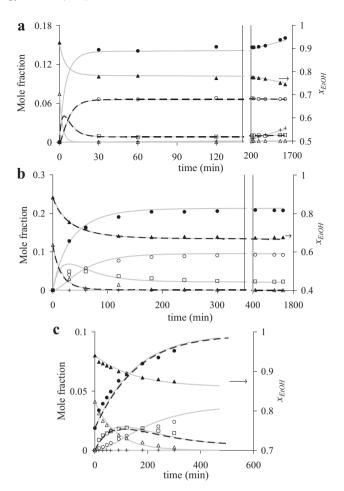
In the application of Eq. (14) to the kinetic parameter regression analysis, n is the number of experimental samples withdrawn from batch reactors in all experiments regressed for each reaction system, and N_C is the number of components considered in each sample. For EtOH etherification and AcAc esterification, all components present were considered in Eq. (8); for SA esterification only the succinate species (SA, MES, DES) were considered.

Final optimized kinetic parameters for Eqs. (10)–(13) along with their 95% confidence intervals, are listed in Table 4. From the optimized constants, the sum of absolute differences f_{ABS} for each model was calculated using Eq. (14); values of f_{ABS} for each experiment are given in Table S3 in the Supplementary information.

3.5. Model comparison with experiment

The kinetic parameters presented in Table 4 agree with those reported for similar catalysts in the literature [21,26–28,34]. Overall, good agreement between model and experimental kinetics is observed at different conditions for simultaneous esterification and etherification.

For EtOH dehydration, both mole fraction and activity-based models predict DEE formation reasonably well (Fig. 5). Only one activity-based predicted profile is presented in Fig. 5 because all others overlap those of the mole fraction model. Experiments at high temperatures (>393 K), high loadings of catalyst ($w_{CAT} > 0.04$) and long reaction time (>500 min) showed significant formation of DEE. At these conditions, flashing of liquid during sampling was observed; this flashing and the resulting change in liquid composition may explain deviation of the model fit from experiment at the most extreme conditions. The large 95% confidence intervals for EtOH dehydration (Table 4) are a consequence of these deviations
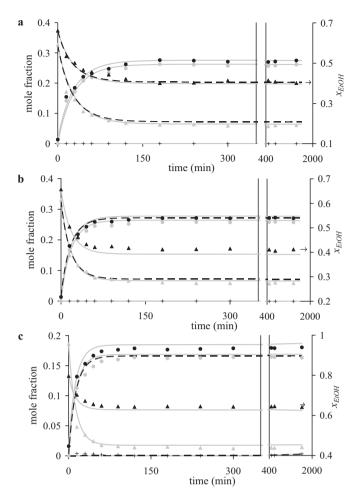

Fig. 6. Experimental and predicted mole fraction profiles in SA esterification. (△) SA; (○) DES; (□) MES; (▲) EtOH; (●) H_2O; (+) DEE; (━━) activity based model; (━━) mole fraction model. (a) Run 27: $T = 379$ K, $w_{CAT} = 0.087$, molar ratio EtOH:SA = 12.5. (b) Run 33: $T = 365$ K, $w_{CAT} = 0.022$, EtOH:SA = 7.49. (c) Run 37: $T = 343$ K, $w_{CAT} = 0.011$, EtOH:SA = 22.8.

of model from experiment at extreme conditions, of the relatively small set of data collected for EtOH dehydration kinetics, and of the so-called "compensation effect," where simultaneously changing pre-exponential factor and activation energy can give essentially the same rate constant over a relatively narrow range of temperatures.

For esterification, experimental results from Runs 27, 33 and 37 for succinic acid and Runs 53, 61 and 78 for acetic acid are presented and compared with kinetic model predictions in Figs. 6 and 7, respectively. Additional kinetic profiles are presented in the Supplementary information. Again, the activity-based kinetic model predictions overlap the profiles obtained from the mole fraction model, so only one set is shown. In general, excess EtOH and high loadings of catalyst ($w_{CAT} > 0.01$) give nearly complete conversion of SA after 2 h of reaction. This time is even shorter at temperatures above 373 K. However, significant quantities of DEE are produced at high temperature. This is clearly observed in Fig. 6a (Run 27), where SA esterification in a large excess of EtOH approaches equilibrium in less than 1 hour, but irreversible diethyl ether (DEE) formation continues to produce additional DEE and eventually shifts the mixture composition from equilibrium. Thus EtOH dehydration to DEE limits the maximum temperature that can be used for ethanol esterification reactions.

The values of the 95% confidence intervals in Table 4 are all relatively small percentages of the values of the rate constants, reflecting both a good fit of the experimental data and a large
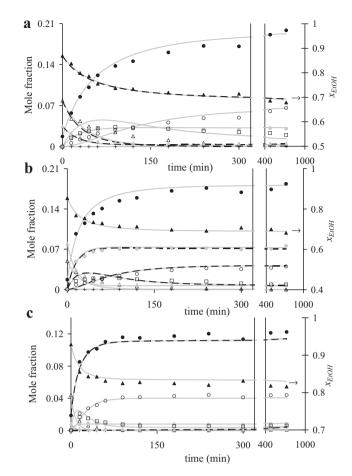
Fig. 7. Experimental and predicted mole fraction profiles in AcAc esterification. (▲) AcAc; (●) EtAc; (▲) EtOH; (●) H_2O; (+) DEE; (━━ ━━) activity based model; (━━) mole fraction model. (a) Run 53: $T = 353$ K, $w_{CAT} = 0.021$, molar ratio EtOH:AcAc = 2.02. (b) Run 61: $T = 363$ K, $w_{CAT} = 0.021$, mole ratio EtOH:AcAc = 1.98. (c) Run 78: $T = 383$ K, $w_{CAT} = 0.011$, mole ratio EtOH:AcAc = 4.29.

Fig. 8. Experimental and predicted mole fraction profiles in mixed SA/AcAc esterification. (▲) AcAc; (●) EtAc; (△) SA; (○) DES; (□) MES; (▲) EtOH; (●) H_2O; (+) DEE. (━━ ━━) activity based model; (━━) mole fraction model. (a) Run 84: $T = 363$ K, $w_{CAT} = 0.011$, mole ratio EtOH:SA = 11.1 and SA:AcAc = 2.2. (b) Run 86: $T = 373$ K, $w_{CAT} = 0.013$, mole ratio EtOH:SA = 17.3 and SA:AcAc = 0.62. (c) Run 88: $T = 363$ K, $w_{CAT} = 0.022$, mole ratio EtOH:SA = 21.1 and SA:AcAc = 5.3.

number of data points. Based on these confidence intervals, we can say that the kinetic constants in Table 4 represent the values that best describe esterification over Amberlyst 70.

The necessity of using a large excess of EtOH in experiments, and the resultant errors arising from analytical uncertainty at the low values of mole fraction for some species, is a consequence of the low solubility of SA (~10 wt% or 23:1 EtOH:SA at 298 K) in alcohol. We ran experiments at higher SA initial concentrations, but the slow dissolution rate and limited solubility of SA at low temperature resulted in undissolved SA in the reactor after reaction started. This led to incomplete closure of the mass balance and a poor fit of the kinetic data at short reaction times. Thus, sampling of experiments with higher SA concentrations was limited to at least 30 min after reaching reaction temperature; no attempt was made to capture the early kinetic behavior of these esterification reactions. Characterizing such early reaction behavior would require handling a predissolved, heated feed solution under pressure, a scenario that we were not prepared to undertake.

Based on a catalyst acid site density of 2.35 meq/g, the initial turnover number for SA esterification over Amberlyst 70 at 353 K and 7.5:1 EtOH:SA molar ratio is 69 h^{-1}. At the same conditions, we have found that more commonly used Amberlyst 15 macroreticular resin has a turnover frequency of 48 h^{-1}. These results agree with the higher acid strength and higher turnover numbers reported for sulfonic groups in chlorinated resins such as Amberlyst 70 [19,39]

and are consistent with higher accessibility (e.g. higher effective diffusivity of reactants) to actives sites in a swelled gel-type structure compared with a macroreticular resin [19].

3.6. Mixed acid esterification

Using the kinetic parameters determined in individual SA and AcAc esterification reactions (Table 4), the modeling of mixed SA and AcAc esterification was performed by integrating Eq. (9) for each species in the mixture. The sum of absolute differences f_{ABS} (Eq. (14)) was calculated and is presented in Table S3 of the Supplementary information. Larger values of f_{ABS} are observed in mixed acid esterification than in AcAc or SA esterification alone, again because the large excess of EtOH used in these experiments gave low initial mole fraction values of acids that declined rapidly as near-complete conversion of both SA and AcAc was achieved. At these conditions, uncertainty in analytical measurements is significant. Nevertheless, the model predicts mixed acid esterification reasonably well, as shown in the kinetic profiles presented in Fig. 8.

Because the simple combination of individual esterification reactions reasonably predicts the mixed acid results, it is apparent that the esterification reactions proceed without competition for catalyst active sites among the acid species. In other esterification studies, a Langmuir–Hinshelwood type expression has often been invoked to describe rate [40,41]. It is clear here that the catalyst active sites are not occupied to a significant degree by either SA

or AcAc, probably because of the large excess of EtOH, and possibly the fact that the first step of esterification is often considered to be protonation of the alcohol by the acid catalyst. Considering that excess EtOH is required to dissolve SA under any conditions, the conditions used in this study will hold at most industrial processing conditions.

The kinetic model obtained here has recently proven successful in the design of a reactive distillation for mixed acid esterification of SA and AcAc with EtOH [42]. Despite recent advances in fermentation that produce SA with high selectivity, other acids can be present for downstream esterification, and this model provides insight into their effect on SA esterification.

4. Conclusions

Mixed acid esterification of SA and AcOH with EtOH was studied using Amberlyst 70 as catalyst. This sulfonic resin showed higher activity as an esterification catalyst than traditional Amberlyst 15, and is better-suited for high temperature use than Amberlyst 15 because of its higher thermal stability. A theoretical and experimental study of intraparticle mass transfer revealed only minor mass transfer resistances at reaction conditions. By performing experiments under different conditions, kinetic models for esterification of SA with EtOH, AcOH with EtOH and etherification of EtOH to DEE were obtained. A linear combination of these individual kinetic models (activity- or mole fraction-based) reproduces experimental data obtained in mixed SA and AcAc esterification with EtOH. This result indicates that mixed acid esterification occurs without competition by acid species for catalyst active sites, and shows that simple, pseudo-homogeneous second order rate expressions are able to describe esterification reaction kinetics reasonably well. The kinetic model described here can be used to design reactive distillation systems for mixed acid esterification of SA and AcAc.

Acknowledgment

Appendix A. Supplementary information

Supplementary information associated with this article can be found, in the online version, at doi:10.1016/j.cej.2012.01.103.

References

[1] C. Potera, Making succinate more successful, Environ. Health Perspect. 113 (12) (2005) A832–A835.
[2] M. Patel, M. Crank, V. Dornburg, B. Hermann, L. Roes, B. Hüsing, L. Overbeek, F. Terragni, E. Recchia, Medium and long-term opportunities and risks of the biotechnological production of bulk chemicals from renewable resources – The potential of white biotechnology (The BREW project), Utrecht, Netherlands, 2006 (online) available: http://www.bio-economy.net/applications/files/Brew_project_report.pdf (June, 2010).
[3] B. Hermann, M. Patel, Today's and tomorrow's bio-based bulk chemicals from white biotechnology, Appl. Biochem. Biotechnol. 136 (2007) 361–388.
[4] J.B. McKinlay, C. Vieille, J.G. Zeikus, Prospects for a bio-based succinate industry, Appl. Microbiol. Biotechnol. 76 (2007) 727–740.
[5] A. Cukalovic, C.V. Stevens, Feasibility of production methods for succinic acid derivatives: a marriage of renewable resources and chemical technology, Biofuels Bioprod. Biorefin. 2 (6) (2008) 505–529.
[6] C. Delhomme, D. Weuster-Botz, F.E. Kühn, Succinic acid from renewable resources as a C4 building-block chemical—a review of the catalytic possibilities in aqueous media, Green Chem. 11 (2009) 13–26.
[7] O. Wolf, M. Crank, M. Patel, F. Marscheider-Weidemann, J. Schleich, B. Hüsing, G. Angerer, Techno-economic feasibility of large-scale production of Bio-based polymers in Europe, European Science and Technology Observatory, EUR 22103 EN, 2005 (online) available: http://ftp.jrc.es/EURdoc/eur22103en.pdf (June, 2010).
[8] I. Bechthold, K. Bretz, S. Kabasci, R. Kopitzky, A. Springer, Succinic acid: A new platform chemical for biobased polymers from renewable resources, Chem. Eng. Technol. 31 (2008) 647–654.
[9] J.G. Zeikus, M.K. Jain, P. Elankovan, Biotechnology of succinic acid production and markets for derived industrial products, Appl. Microbiol. Biotechnol. 51 (1999) 545–552.
[10] L. Agarwal, J. Isar, R. Saxena, Rapid screening procedures for identification of succinic acid producers, J. Biochem. Biophys. Methods 63 (2005) 24–32.
[11] P. Rogers, J. Chen, M. Zidwick, The prokaryotes, Organic Acid and Solvent Production, Part I: Acetic, Lactic, Gluconic, Succinic and Polyhydroxyalkanoic Acids, 2006 511–755, Chapter 3.1.
[12] H. Song, S.Y. Lee, Production of succinic acid by bacterial fermentation, Enzyme Microb. Technol. 39 (2006) 352–361.
[13] A. Orjuela, A.J. Yanez, C.T. Lira, D.J. Miller, Carboxylic Acid Recovery from Fermentation Solutions, US Patent Application Prov. Appl. Serial No. 61/265,851, 2009, Filed 2009.
[14] C. Bianchi, A new method to clean industrial water from acetic acid via esterification, Appl. Catal. B 40 (2) (2003) 93–99.
[15] D. Sutton, G. Reed, A.G. Hiles, Process for the production of esters of mono-, di or polycarboxylic acids, WO patent 051885 A1, U.S. Patent Application 20070129565A1, 2007.
[16] W. Zhao, X. Sun, Q. Wang, H. Ma, Y. Teng, Lactic acid recovery from fermentation broth of kitchen garbage by esterification and hydrolysis method, Biomass Bioenergy 33 (1) (2009) 21–25.
[17] R. Bringué, M. Iborra, J. Tejero, J.F. Izquierdo, F. Cunill, C. Fité, V.J. Cruz, Thermally stable ion-exchange resins as catalysts for the liquid-phase dehydration of 1-pentanol to di-n-pentyl ether (DNPE), J. Catal. 244 (2006) 33–42.
[18] R. Bringué, J. Tejero, M. Iborra, J.F. Izquierdo, C. Fité, F. Cunill, Water effect on the kinetics of 1-pentanol dehydration to di-n-pentyl ether (DNPE) on Amberlyst 70, Top. Catal. 45 (1–4) (2007) 181–186.
[19] P.F. Siril, H.E. Cross, D.R. Brown, New polystyrene sulfonic acid resin catalysts with enhanced acidic and catalytic properties, J. Mol. Catal. A. Chem. 279 (2008) 63–68.
[20] Rohm, Haas, Amberlyst 70 product data sheet. Philadelphia, USA. (2005).
[21] A. Kolah, N. Asthana, D. Vu, C.T. Lira, D.J. Miller, Reaction kinetics for the heterogeneously catalyzed esterification of succinic acid with ethanol, Ind. Eng. Chem. Res. 47 (15) (2008) 5313–5317.
[22] D.J. Miller, N. Asthana, A. Kolah, D. Vu, C.T. Lira, Process for reactive esterification distillation, US Patent 7,667,068 (2006).
[23] A. Darlington, W. Guenther, Ethanol–acetic acid esterification equilibrium with acid ion-exchange resin as catalyst, J. Chem. Eng. Data 12 (4) (1967) 605–607.
[24] J. Gimenez, S. Cervera-March, Catalytic activity of sulfonated styrene - divinylbenzene resins, Appl. Catal. 48 (2) (1989) 307–332.
[25] M. Mazzotti, B. Neri, D. Gelosa, A. Kruglov, M. Morbidelli, Kinetics of liquid-phase esterification catalyzed by acidic resins, Ind. Eng. Chem. Res. 36 (1) (1997) 3–10.
[26] G. Hangx, G. Kwant, H. Maessen, P. Markusse, I. Urseanu, Reaction Kinetics of the Esterification of Ethanol and Acetic Acid Towards Ethyl Acetate, Deliverable 22, Intelligent Column Internals for Reactive Separations (INTINT). Technical Report to the European Commission (2001), (online) available: http://www.cpi.umist.ac.uk/intint/NonConf_Del/22.pdf (June, 2010).
[27] Ş. Kirbaşlar, Z. Baykal, U. Dramur, Esterification of acetic acid with ethanol catalyzed by an acidic ion-exchange resin, Turk. J. Eng. Environ. Sci. 25 (2001) 569–577.
[28] N. Calvar, B. Gonzalez, A. Dominguez, Esterification of acetic acid with ethanol: reaction kinetics and operation in a packed bed reactive distillation column, Chem. Eng. Process. 46 (2007) 1317–1323.
[29] I. Lai, Y. Liu, C. Yu, M. Lee, H. Huang, Production of high-purity ethyl acetate using reactive distillation: experimental and start-up procedure, Chem. Eng. Process. 47 (2008) 1831–1843.
[30] T. Dogu, E. Aydiny, N. Bozz, K. Murtezaoglu, G. Doguyy, Diffusion Resistances and contribution of surface diffusion in TAME and TAEE production using Amberlyst-15, Int. J. Chem. React. Eng. 1 (A6) (2003) 1–10.
[31] P.B. Weisz, C.D. Prater, Interpretation of measurements in experimental catalysis, Adv. Catal. 6 (1954) 143–196.
[32] H. Renon, J.M. Prausnitz, Local composition in thermodynamic excess functions for liquid mixtures, AIChE J. 14 (1968) 135–144.
[33] Aspentech, Aspen Physical Property System, physical property models/methods, Burlington, 2007.
[34] Y. Tang, H. Huang, I. Chien, Design of a complete ethyl acetate reactive distillation system, J. Chem. Eng. Jpn. 36 (11) (2003) 1352–1366.
[35] A. Orjuela, A.J. Yanez, D. Vu, D. Bernard-Brunel, D.J. Miller, C.T. Lira, Phase equilibria for reactive distillation of diethyl succinate: Part I. System diethyl succinate + ethanol + water, Fluid Phase Equilib. 290 (2010) 63–67.
[36] A. Orjuela, A.J. Yanez, P. Rossman, D. Vu, D. Bernard-Brunel, D.J. Miller, C.T. Lira, Phase equilibria for reactive distillation of diethyl succinate. Part II: Systems diethyl succinate + ethyl acetate + water and diethyl succinate + acetic acid + water, Fluid Phase Equilib. 290 (2010) 68–74.
[37] A. Orjuela, A.J. Yanez, J. Evans, D.J. Miller, C.T. Lira, Phase equilibria in binary mixtures with monoethyl succinate, Fluid Phase Equilib. 309 (2011) 121–127.
[38] A. Orjuela, A.J. Yanez, A. Lee, D.J. Miller, C.T. Lira, Solubility and Phase Equilibria for Mixtures with Succinic Acid, under review (2011).

[39] J.R. Collin, D. Ramprasad, Methods, systems and catalysts for the hydration of olefins, European patent application EP 1479665 A1.

[40] T. Pöpken, L. Götze, J. Gmehling, Reaction kinetics and chemical equilibrium of homogeneously and heterogeneously catalyzed acetic acid esterification with methanol and methyl acetate hydrolysis, Ind. Eng. Chem. Res. 39 (7) (2000) 2601–2611.

[41] H.T.R. Teo, B. Saha, Heterogeneous catalyzed esterification of acetic acid with isoamyl alcohol: kinetic studies, J. Catal. 228 (2004) 174–182.

[42] A. Orjuela, A. Kolah, C.T. Lira, D.J. Miller, Mixed succinic acid/acetic acid esterification with ethanol by reactive distillation, Ind. Eng. Chem. Res. 50 (2011) 9209–9220.